Stem Cell Reports
Article

ISSCR

OPEN ACCESS

Histone H3 K4/9/27 Trimethylation Levels Affect Wound Healing and Stem Cell Dynamics in Adult Skin

Sangjo Kang,[1] Kylie Long,[1,3] Sherry Wang,[1,3] Aiko Sada,[1,2] and Tudorita Tumbar[1,*]
[1]Department of Molecular Biology and Genetics, Cornell University, Ithaca, NY 14853, USA
[2]International Research Center for Medical Sciences, Kumamoto University, Kumamoto City 860-0811, Japan
[3]Co-second authors
*Correspondence: tt252@cornell.edu
https://doi.org/10.1016/j.stemcr.2019.11.007

SUMMARY

Epigenetic mechanisms controlling adult mammalian stem cell (SC) dynamics might be critical for tissue regeneration but are poorly understood. Mouse skin and hair follicle SCs (HFSCs) display reduced histone H3 K4me3, K9me3, and K27me3 methylation levels (hypomethylation) preceding hair growth. Chemical inhibition of relevant histone demethylases impairs subsequent differentiation and growth of HFs and delays wound healing. In wounding, this impairs epithelial cell differentiation and blood vessel recruitment, but not proliferation and fibroblast recruitment. With *Aspm*-CreER as a newfound inter-follicular epidermis lineage-labeling tool, and *Lgr5*-CreER for hair follicles, we demonstrate a reduced contribution of both lineages to wound healing after interfering with hypomethylation. Blocked hypomethylation increases BMP4 expression and selectively upregulates H3 K4me3 on the *Bmp4* promoter, which may explain the effects on HFSC quiescence, hair cycle, and injury repair. Thus, transient hypomethylation of histone H3 K4/9/27me3 is essential for adult skin epithelial SC dynamics for proper tissue homeostasis and repair.

INTRODUCTION

The stem cell (SC) genome is highly plastic, allowing rapid changes in global gene expression patterns to self-renew and differentiate, adopting different cell fates. In embryonic SCs, genome plasticity is influenced by special epigenetic states, with specific patterns and levels of histone H3 K4me3, K9me3, and K27me3 (H3 K4/9/27me3). In particular, global hypomethylation of histone H3 K9/27me3, two transcriptional repressive marks, regulate embryonic SC plasticity (Boyer et al., 2006; Chen et al., 2013; Hawkins et al., 2010; Jiang et al., 2011; Loh et al., 2007; Mattout and Meshorer, 2010; Meshorer et al., 2006).

Tissue SC behavior and cell fate acquisition, or "SC dynamics," are critical for tissue regeneration in both normal homeostasis and injury repair, and must be tightly linked with genome plasticity. However, mechanisms of adult tissue SC genome plasticity are poorly understood *in vivo*, due to SC scarcity and inaccessibility to their niche (Avgustinova and Benitah, 2016; Blanpain and Fuchs, 2014). Importantly, many tissue SCs (e.g., muscle, blood, and hair follicle) are quiescent before cell fate changes (Fuchs, 2009). Intriguingly, hypomethylation of histone H3 K9/27me3 correlates with quiescence in muscle SCs *in vivo* and T cells *in vitro* (Baxter et al., 2004; Liu et al., 2013). Furthermore, hypomethylation is required for genome plasticity of quiescent T cells (Baxter et al., 2004). Recently, we showed hypomethylation of quiescent hair follicle (HF) SCs of H3 K9/27me3 and also of H3 K4me3 marks (Lee et al., 2016). Hypomethylation occurs at a stage of hair homeostasis (hair cycle) known as Catagen (Kang et al., 2019; Lee et al., 2016), which precedes HFSC fate determination occurring at Telogen, when HFSC either locate in their niche (bulge) or in the activation/differentiation zone known as hair germ (Hsu et al., 2011; Lee et al., 2013). Location determines subsequent cell fate, finalized by Anagen, when cells in the bulge self-renew while the hair germ proliferate and irreversibly differentiate to matrix progenitors and further to hair shaft. Because cell fate is undetermined in Catagen, it follows that cells must likely be characterized by highest genome plasticity (Sada and Tumbar, 2013). Similar with embryonic SCs, the catagen hypomethylation of HFSCs might allow high plasticity, or flexibility in subsequent SC fate acquisition (Figure 1A). In fact, we found that other measurements of plasticity, such as dynamic exchange of chromatin-bound factors, and reprogramming ability by the Yamanaka 4F factors are also elevated at Catagen (Lee and Tumbar, 2017).

We demonstrated that interfering with hypomethylation at Catagen in adult skin can affect HFSC activation and the onset of hair growth (Lee et al., 2016). It remained unclear whether hypomethylation effect on hair growth is stage specific, and whether it is relevant to hair cycle stages beyond SC activation and to wound healing. To address these questions, here we block H3 K4/9/27me3 hypomethylation by applying histone demethylase inhibitors (DIs) to adult mouse skin at different hair cycle stages. Hypomethylation at late Anagen/Catagen proved relevant for subsequent skin repair of punch wounds, specifically acting on keratinocyte differentiation and recruitment of blood vessels, but not on keratinocyte proliferation or recruitment of fibroblast. We studied hypomethylation effect on behavior of two SC populations located either in the inter-follicular epidermis (IEF) or the HF. We characterize

 © 2019 The Author(s).
This is an open access article under the CC BY-NC-ND license (http://creativecommons.org/licenses/by-nc-nd/4.0/).

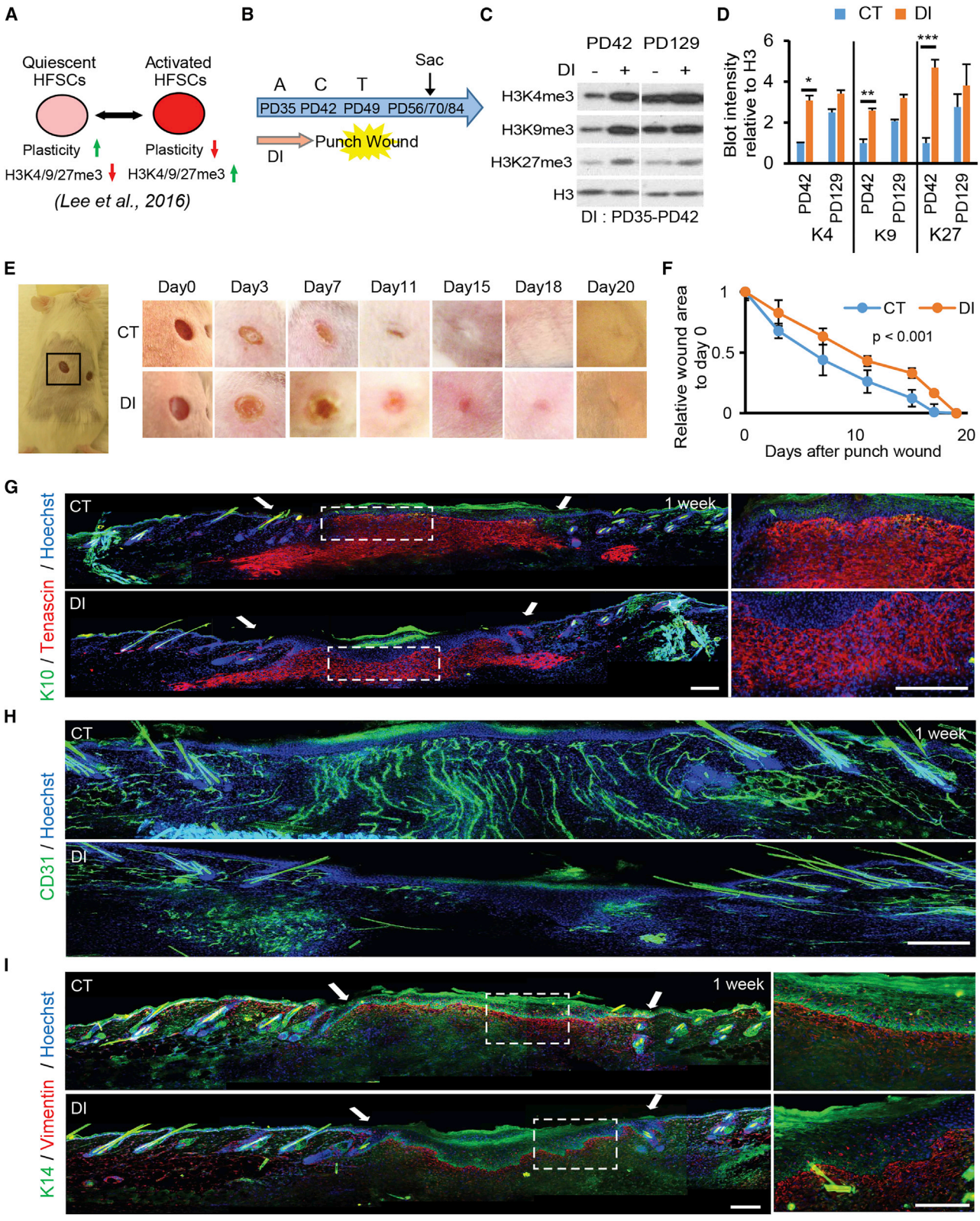

(legend on next page)

abnormal spindle microtubule assembly (*Aspm*)-CreER mice (Marinaro et al., 2011) for their induction in the skin and demonstrate robust labeling in the inter-follicular epidermis (IFE), which provides new genetic tools for skin targeting. We use the *Lgr5*-CreER, as a known driver in the HFSC lineage to examine effect of methylation level on HF contribution to wound healing (Jaks et al., 2008). We find that interfering with hypomethylation affects migration and contribution to wound healing of both IFE and HF lineages. Hypomethylation was relevant to HFSC activation timing, as reported (Lee et al., 2016), but here we show that HFs eventually grow, albeit with transient defects in differentiation. Hypomethylation interference and subsequent hair growth defects are hair cycle stage dependent and do not occur at anagen; Hypomethylation also affects the levels of BMP4 expression. BMP-signaling controls hair cycle progression, HFSC activation and differentiation (Botchkarev and Sharov, 2004; Lee and Tumbar, 2012), and also acts in wound healing (Lewis et al., 2014a). BMP4 elevation in skin correlates with selective increase of activating mark H3 K4me3 (but not of H3 K9/27me3) on the *Bmp4* promoter in response to hypomethylation interference. Thus, hair cycle-specific H3 K4/9/27me3 hypomethylation is relevant for IFE and HFSC function in homeostasis and wound healing, likely in part through BMP signaling. We provide a model and general road map for future genetic studies of histone methylation role in the skin and for clinical investigation.

RESULTS

Impaired Hypomethylation Delays Skin Wound Healing

To examine histone H3 K4/9/27me3 hypomethylation relevance to wound healing, we applied DIs to mouse back skin at late Anagen/Catagen (postnatal day [PD]35–42) when hypomethylation is strong (Lee et al., 2016) (Figure 1B). These DIs have been shown to target specifically the H3 K4 and K9 de-methylases (JIB 04) and K27 demethylases (GSK J1) (Kruidenier et al., 2012; Lee et al., 2016; Wang et al., 2013), and induced H3 K4/9/27me3 elevation through later stages (Figures 1C, 1D, S1A, and S1B), as expected. Next, we applied a punch wound at PD49, and measured delayed wound area closure relative to the original wound size (Figures 1E and 1F). Next, we examined specific cellular processes important in wound healing. Expression of spinous layer differentiation markers keratin 1 and 10 was decreased in the DI-treated wounded skin relative to control while the basal layer (BL) markers K14 and α6-integrin were maintained (Figures 1G, S1C, and S1D). Proliferation of BL cells, indicated by Ki67 staining, was not affected (Figure S1D). In addition to keratinocytes, blood vessels and fibroblasts from the nearby dermis are also recruited to the wounded site (Martin and Leibovich, 2005). Strikingly, vascularization as determined by CD31 staining, was extremely delayed in DI-treated skin wounds (Figures 1H and S1E), whereas, fibroblast recruitment determined by vimentin staining was normal (Figure 1I). Thus, impairing hypomethylation during Catagen delays injury repair along with epidermal differentiation and blood vessel recruitment, but not epidermal proliferation and fibroblast recruitment at the wound site.

Aspm-CreER Genetic Tools to Mark the IFE BL SCs

Subsequently, we wanted to examine whether H3 K4/9/27me3 levels may differentially affect contributions to wound healing from SC populations of the HF versus the IFE. For this, we employed genetic lineage tracing tools using tamoxifen (TM) inducible CreER recombinase that marks specifically SCs in the HF via *Lgr5*-CreER (Jaks et al., 2008) (Figure 2A). For the IFE, we tested a potential driver *Aspm*-CreER (Marinaro et al., 2011) that surfaced as

Figure 1. Injury Repair Is Delayed after Demethylase Inhibitor Application in Mouse Back Skin during Late Anagen/Catagen

(A) Scheme of cellular plasticity and methylation levels in quiescent and activated HFSCs.

(B) Scheme of demethylase inhibitor (DI) application and the punch wound experiment. A, Anagen; C, Catagen; T, Telogen; PD, postnatal day.

(C) Western blots for control vehicle (CT) or DI applied to wild-type mice during late Anagen/Catagen (PD35-42) phase and sacrificed at the ages indicated at top. For the whole blot, see Figure S1A.

(D) Quantification of the western blots in (B and S1A). Three mice were used per time point for statistical analysis. *p = 0.005, **p = 0.005, ***p = 0.009.

(E) Punch wound pictures of (PD35-42) CT- or DI-treated mice at different days after the punch wound.

(F) Punch wound size measurements on images like those in (E). N = 5 mice per group. ANOVA was used for significance test.

(G) Tenascin and K10 staining skin sections including the punch wound of wild-type mice after CT or DI application 1 week after the wound. Panels on the left are enlargements of corresponding white dotted line insets on the right.

(H) Blood vessel (CD31) and DNA (Hoechst) staining in 1-week punch wound skin sections of wild-type mice after CT or DI application. Arrows indicate the wound edges at the junction with normal skin.

(I) Fibroblast (vimentin) and K14 staining in 1-week punch wound skin sections of wild-type mice after CT or DI application. Arrows indicate the wound edges at the junction with normal skin.

Student's t test was used for all significance tests except (F). All the experiments were executed twice. Scale bars, 20 μm.

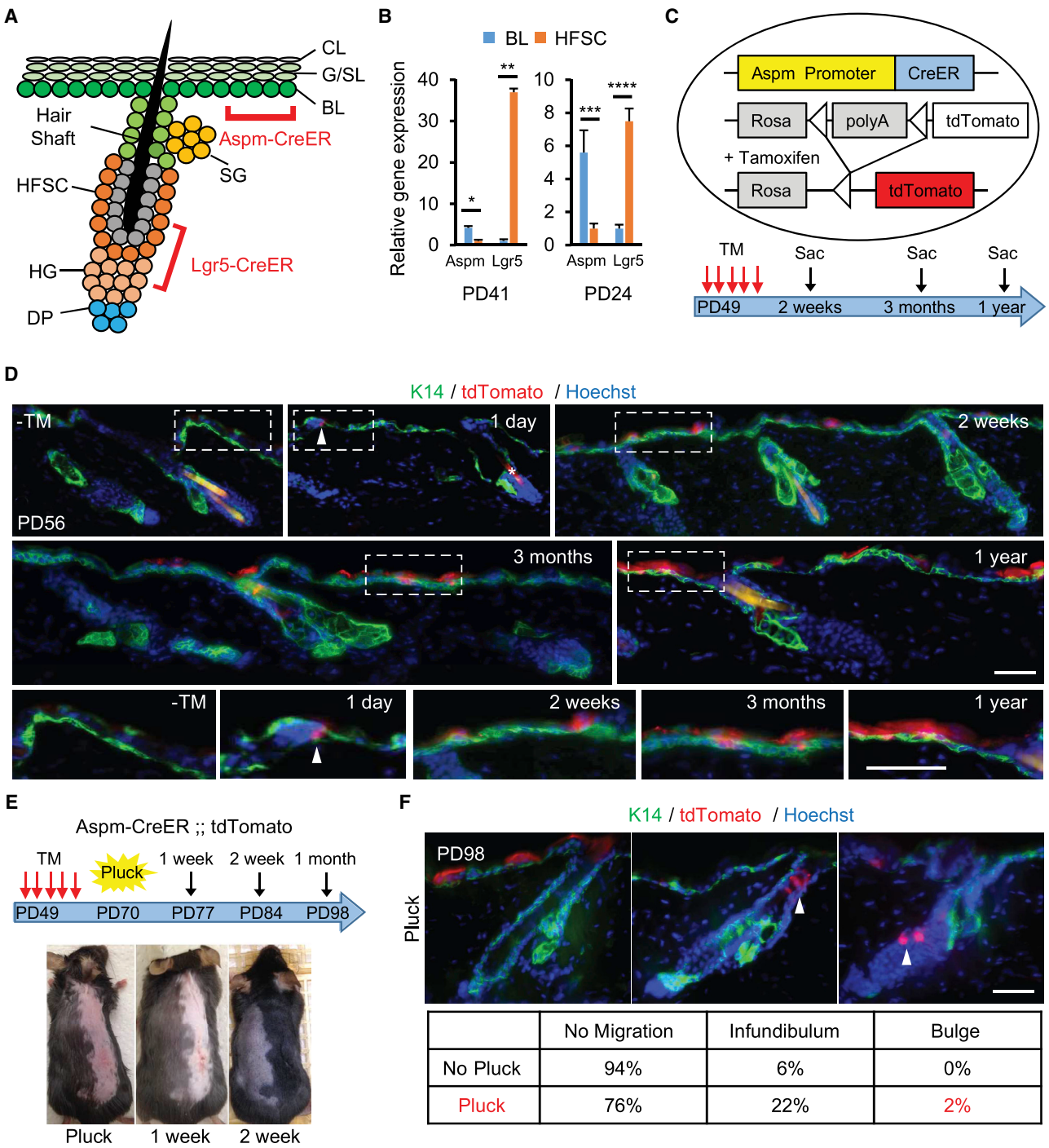

	No Migration	Infundibulum	Bulge
No Pluck	94%	6%	0%
Pluck	76%	22%	2%

Figure 2. Lineage Tracing of Inter-Follicular Epidermis Stem Cells in Aspm-CreER Mice

(A) Scheme of the epithelial skin structure with epidermis at the top and HF at the bottom. CL, cornified layer; G/SL, granular/spinous layer; BL, basal layer; SG, sebaceous gland; HFSC, HF stem cell; HG, hair germ; DP, dermal papilla. Note the marking of epidermis versus HF using *Aspm*-CreER versus *Lgr5*-CreER genetic drivers.

(B) Gene expression analysis of FACS-sorted inter-follicular epidermis (IFE) BL cells and HFSCs in Catagen (PD41) and Anagen (PD24). N = 3 of biological replicates; *p = 0.009, **p = 0.0002, ***p = 0.017, ****p = 0.001. HFSCs are FACS sorted as α6-integrin+/CD34+ and BL cells were α6-integrin+/CD34− cells. Student's t test was used for all significance tests.

(legend continued on next page)

a specific candidate of IFE marker not found in the HF, from our previous microarray analysis (Sada et al., 2016) (Figure 2A). The differential expression of *Lgr5* and *Aspm* markers in HFSCs and epidermal BL cells was first confirmed by qRT-PCR analysis of fluorescence-activated cell sorting (FACS)-sorted CD34+/α6-integrin+ as HFSCs and CD34−/α6-integrin+ as BL-enriched cells (Figure 2B).

To test the *Aspm*-CreER-marked cells for their localization and contribution to skin homeostasis, we used the Rosa26-tdTomato reporter mice (Madisen et al., 2010) induced with TM at PD28 (Figure 2C). We found that at 1 day and 2 weeks after TM injection, abundant tdTomato+ cells were present in the IFE and were excluded from the HFs (Figure 2D). To ask if the *Aspm*-CreER-marked IFE cells possess long-term SC potential, we lineage traced these cells up to 1 year (Figure 2C, bottom). By 3 months, tdTomato *Aspm*-CreER-marked progeny survived and proliferated in the BL, and were present in the suprabasal (differentiated) layers (Figure 2D). By 1 year, they formed frequent large multiple-cell clones in the IFE, with rare marking of the infundibulum (∼6% of HFs) and no marking in the lower HF (Figures 2D and 2F). To further characterize the potential of *Aspm*-CreER-marked cells, we plucked the back skin hair (Figure 2E) and found little, if any, contribution to HFs bellow the infundibulum area (Figures 2E, 2F, and S2). Taken together, these results suggest that *Aspm*-CreER marks specifically and efficiently the IFE and its SCs, away from the HF, and is thus a valuable tool to study long-term behavior of IFE lineages in adult skin without influence from HF phenotypes.

Impaired Hypomethylation Affects IFE SC Contribution to Wound Healing

Next, we asked if *Aspm*-CreER/Rosa26-tdTomato-marked IFE cells contribute to wound healing and if DI affects this contribution (Figure 3A). We injected TM once at PD28 and applied DIs (PD35-42) on back skin to block hypomethylation. After a week (PD49), we apply a punch wound and examined the tdTomato-marked progeny cells (Figure 3B). Similar to previous experiments, wound closure was delayed by DIs (Figures 3C and 3D). Prominent tdTomato trails in the punch wound area, indicated robust contribution of *Aspm*-CreER IFE cells to injury repair in normal but not DI-treated skin (Figures 3E–3G). Interestingly, *Aspm*-CreER-marked cells contributed substantially to HF regeneration near the injury site, both in CD34+ HFSCs and bulge inner layer (Figures S3A–S3C). This differed from lack of contribution to HFs in the plucking experiment (Figure 2F). This suggested that punch wounds deliver a strong incentive to the IFE cells to trans-differentiate to HF. This "trans-differentiation" was modestly, if at all affected by our DI treatment (Figures S3D and S3E). Taken together, our data demonstrate that IFE SC migration and contribution to wound healing is impaired when hypomethylation of skin is blocked prior to injury.

Impaired Hypomethylation Affects the HFSC Contribution to Wound Healing

Next, we asked if *Lgr5*-CreER (Jaks et al., 2008), Rosa26-tdTomato-marked HFSC progeny cells contribute to wound healing in our assay, and if DI affects this (Figures 4A and 4B). In control mice, *Lgr5*-CreER HFSC progeny migrated and differentiated into basal and suprabasal epidermis forming prominent tdTomato+ trails at 1, 3, and 5 weeks post-wound (Figures 4C–4F). However, in DI-treated skin, tdTomato+ cells from the HF migrated much less, and remained confined to the bulge (Figures 4C–4F). These data suggest that hypomethylation at late Anagen/Catagen is relevant to subsequent HFSC progeny migration and contribution to epidermis injury repair.

Histone H3 K4/9/27me3 Hypomethylation of Skin Is Significant for Subsequent Hair Growth and Differentiation

Quiescent HFSCs are activated by wounding and enter a new growth phase, and this growth rapidly spreads away from the wound (controls in Figures 5A and 5B). Blocking hypomethylation with DIs at late Anagen/Catagen (PD35-42), when HFSCs enter quiescence and methylation marks are erased, delayed hair cycle progression up to PD98 (Lee et al., 2016). Here, we examined hair growth in wounds and at time points past PD98, investigate possible

(C) Scheme of lineage tracing using *Aspm*-CreER;Rosa26-tdTomato mice after tamoxifen (TM) injection (red arrows) and different experimental endpoints (black arrowhead); 'sac' stands for time of sacrifice.
(D) Back skin of *Aspm*-CreER;tdTomato mice treated as shown in (C) at endpoints indicated. Arrowhead shows *Aspm*-CreER-marked cells positive for tdTomato. Asterisk indicates autofluorescence from the hair shaft. N = 2 for TM−; N = 3 for the rest of the time points.
(E) Experimental scheme and whole-mouse pictures showing back skin hair plucking of *Aspm*-CreER;tdTomato mice at time points indicated. Note that the right-hand side was plucked, and the hairs grew back by 2 weeks post-plucking. N = 3.
(F) Lineage tracing of *Aspm*-CreER-marked positive IFE cells at PD98, 1 month after plucking. Left panel shows no migration in the HFs. Middle panel shows migration of Aspm cells to the infundibulum (arrowhead). Right panel shows migration of Aspm cells to the bulge (arrowhead). N = 3. The table was generated from averaging 100 HFs from 3 mice at 1 month after hair plucking.
Scale bars, 20 μm.

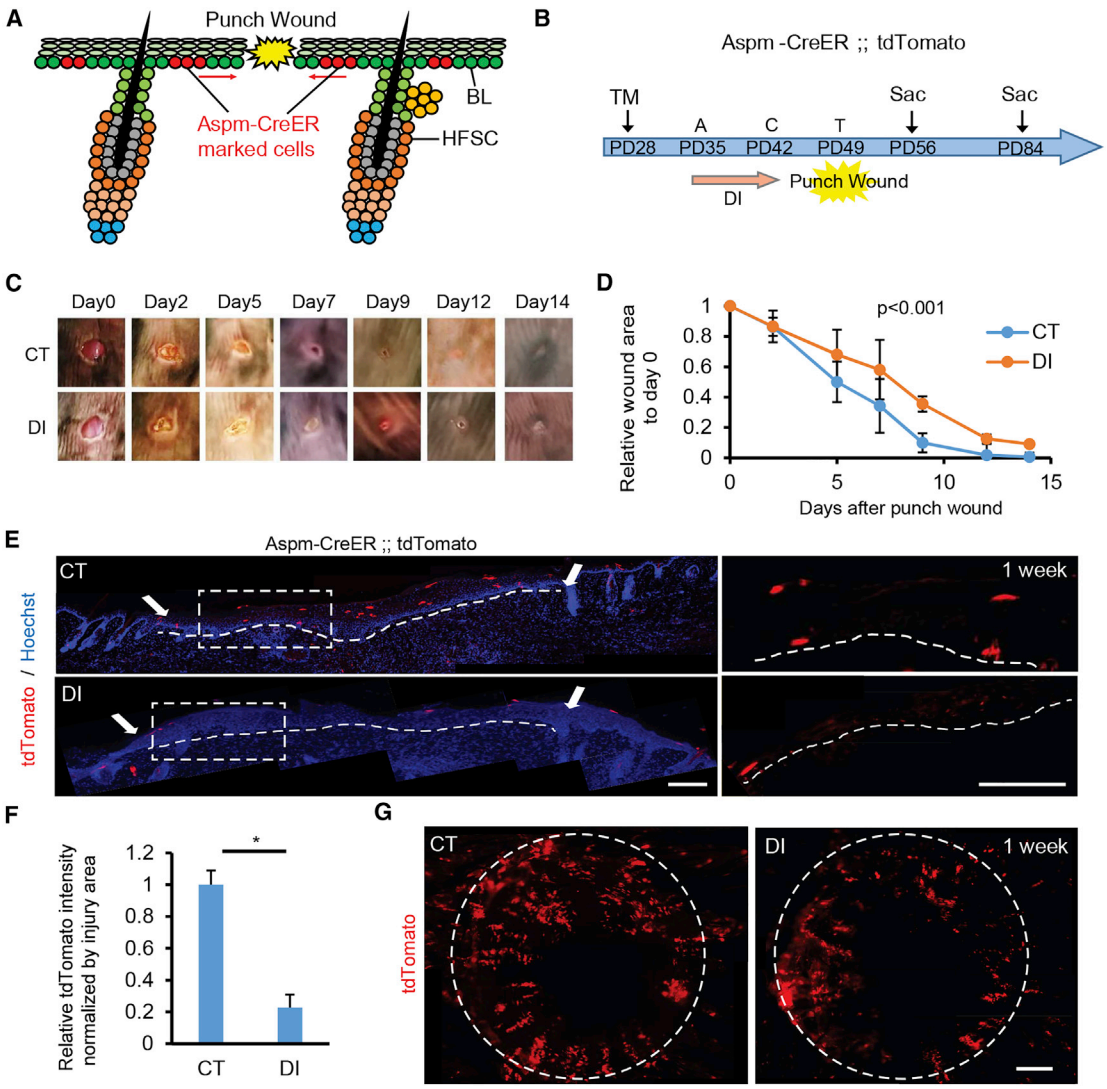

Figure 3. Epidermal Stem Cell Contribution to Wounding Is Impaired by Blocking Hypomethylation at Late Anagen/Catagen

(A and B) Scheme of the *Aspm*-CreER;tdTomato mouse punch wound (A) with the experimental timeline (B).

(C) Pictures of (PD35-42) CT- or DI-treated *Aspm*-CreER;tdTomato mice at different days after the punch wound.

(D) Punch wound size measurement in (C). N = 3 mice per group. ANOVA was used for the significance test.

(E) Sections of skin containing a punch wound 1 week after wounding. Arrows indicate the wound edge neighboring normal skin. Note the prominent trails of tdTomato+ cells in CT skin.

(F) Quantification of the tdTomato signals in the wounded area at 1 week. N = 3; p = 0.0007.

(G) Confocal images of the wounded region after 1 week of the wound. White dashed lines indicate the injury site. N = 3.

Student's t test was used for the significance test in (F). Scale bars, 20 μm.

effects on differentiation, and ask if DI activity is hair cycle stage dependent.

In wounds, hair growth occurred in all mice but its spreading in neighboring regions was delayed by DI treatment (Figures 5A and 5B). Second, HF growth was arrested at Telogen in DI-treated skin away from wounds, in line with previous report that normal hair growth is delayed by DI (Lee et al., 2016). Eventually, hair shafts appeared fully grown in most back skin regions by ~PD129 (Figures 5C and 5D); thus, HF growth impairment induced by blocking hypomethylation at the late Anagen/Catagen is eventually overcome. To investigate if the hair cycle stage at which we inhibit hypomethylation is important for subsequent hair growth, we applied DIs during Anagen (PD28-35), where HFSCs are proliferative (Figure 5C, green arrow). Interestingly, applying DIs at Anagen (PD28-35) did not

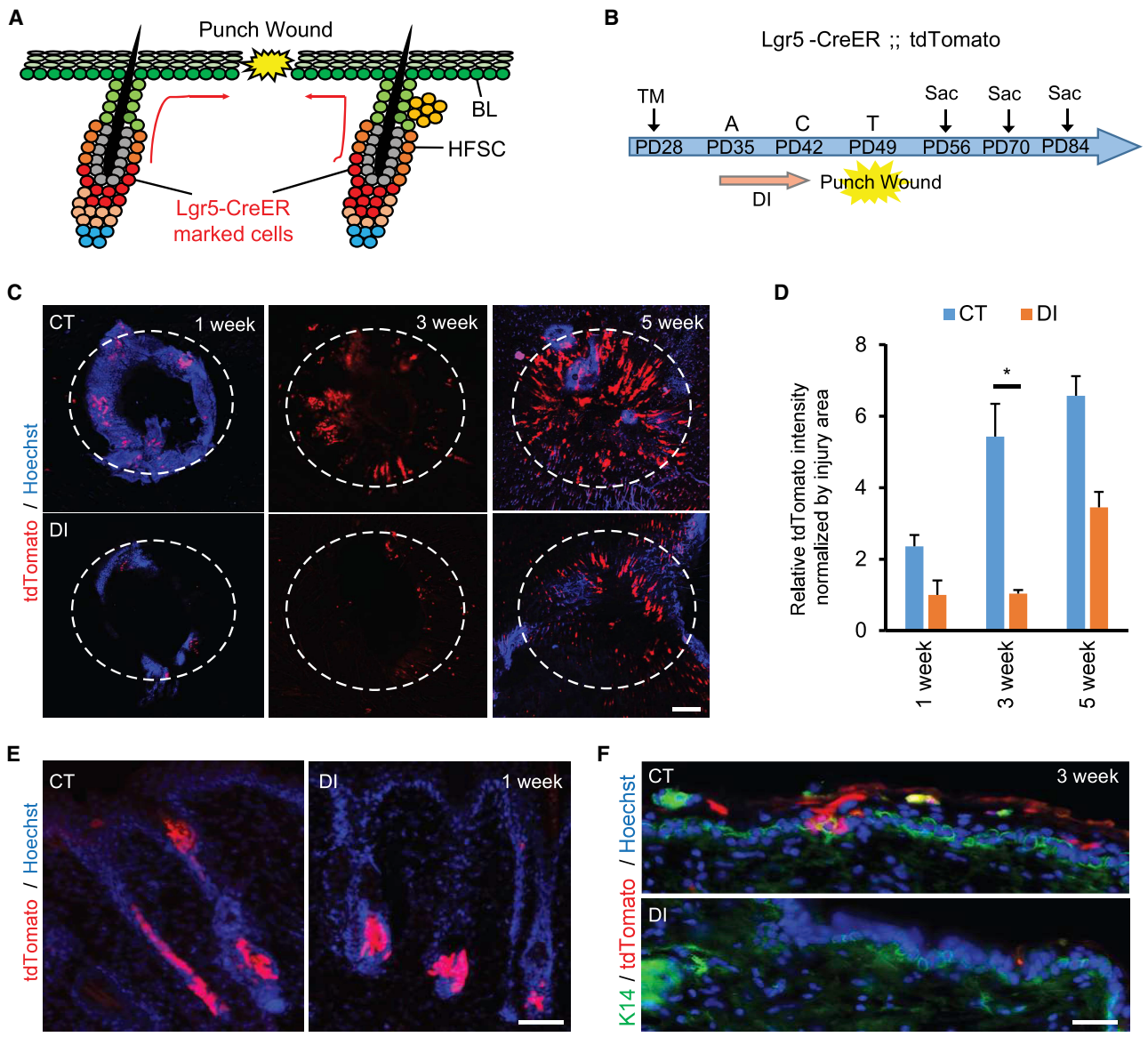

Figure 4. Hair Follicle Stem Cell Contribution to Wounding Is Impaired by Blocking Hypomethylation at Late Anagen/Catagen

(A and B) Scheme of the *Lgr5*-CreER;tdTomato mouse punch wound experiment (A) with the experimental timeline (B).

(C) Confocal images of the wounded region 1, 3, and 5 weeks after the punch wound. White dashed lines indicate the injury site. For 1 and 5 weeks, N = 2; for 3 weeks, N = 3.

(D) Quantification of the Lgr5 lineage traced signals inside the wound region. *p = 0.015. Student's t test was used for the significance test.

(E) Skin sections 1 week after the punch wound shows *Lgr5*-CreER;tdTomato-marked cells trailing from the HF bulge toward the epidermis.

(F) Skin sections of the wounded area 3 weeks after the punch wound. Note prominent tdTomato+ cells present in CT skin, indicating the contribution of HF stem cells to injury and negative effects in DI-treated skin. Scale bars, 20 μm.

affect the skin histone methylation levels nor the hair growth, as seen before with late Anagen/Catagen (PD35-42) applications (Figures 5C, 5E–5G, and S4A). This suggested a hair cycle stage-dependent activity of histone H3 demethylases, confined to late Anagen/Catagen.

Previously, we showed a delay in proliferation onset in the hair germ in mouse skin treated with DIs at PD35-42 and stained with Ki67 and sacrificed at PD56 (Lee et al., 2016). Here, we show by Ki67 staining that DI-treated skin was at early Anagen at PD98 and at Anagen in

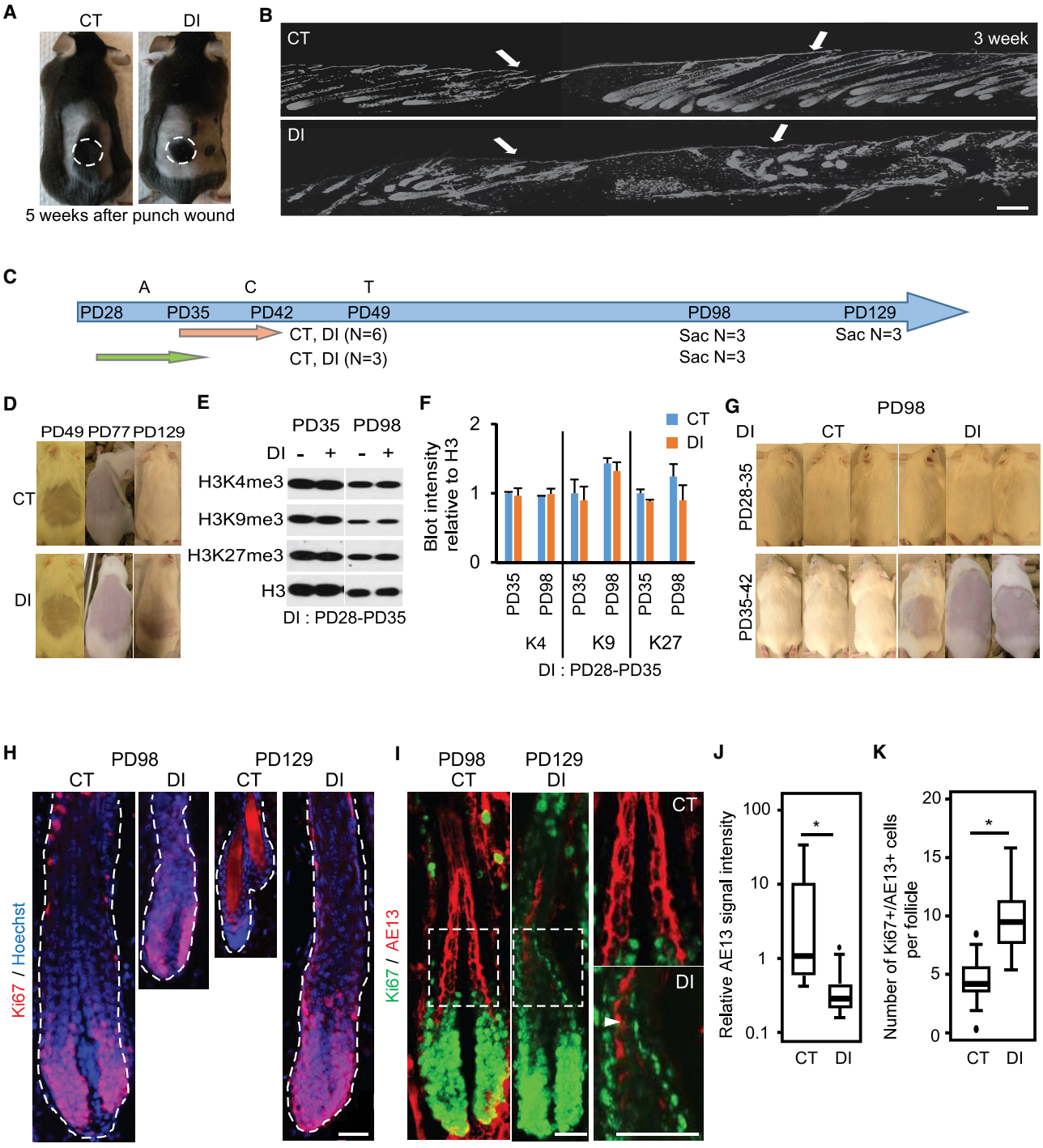

Figure 5. Hair Growth Is Delayed and Hair Differentiation Is Impaired by Blocking Hypomethylation at Late Anagen/Catagen, but Not at Anagen

(A) Whole view of mice 5 weeks after the punch wound. Note the restricted hair growth in the punch wound area in a DI-treated mouse (right panel) and spreading away from the wound area in a CT mouse (left panel).

(B) Skin sections of the wounded area from CT- or DI-treated mice 3 weeks after wounding. Note the Anagen morphology in HFs near the wound edge spreading further into the neighboring regions in CT- but not DI-treated mice.

(C) Experimental scheme with DI treatment at Anagen (green arrow) or late Anagen/Catagen (orange arrow) and timeline with the number of mice analyzed for CT- or DI-treated wild-type mice.

(legend continued on next page)

PD129, whereas control skin was at full Anagen and Telogen, respectively (Figure 5H). Interestingly, DI-treated HFs displayed abnormal morphology, with an uncharacteristic narrow bulb (Figure 5H), not accompanied by detectable apoptosis or DNA damage response (Figure S4B and data not shown), suggesting possible defects in the production of inner differentiated layers. This possibility was supported by decreased AE13 expression (Figures 5I and 5J). Furthermore, we detected more AE13+ cells that also proliferate (Ki67+), normally a rare occurrence (Figures 5I and 5K), and outer-root sheet in hair bulb also proliferated more (Figures S4C and S4D). In conclusion, here we demonstrate that interfering with hypomethylation at late Anagen/Catagen delays Anagen onset, followed by an abnormal pattern of differentiation and proliferation at Anagen. The HFs eventually grow mature hair shafts. Importantly, we also demonstrate that DI treatment does not work at Anagen in perturbing methylation levels in HFs, and in affecting hair growth. This effect is specific to late Anagen/Catagen, the stage when HFSCs enter quiescence and hypomethylation is apparent (Lee et al., 2016). This suggests that it is selectively at this stage when demethylases act in skin and HFs.

Histone H3 K4/9/27me3 Levels Act on BMP Signals

Next, we wondered how interfering with histone methylation level at late Anagen/Catagen may result in hair cycle defects and delays in epithelial cell migration and differentiation during injury repair. BMP signaling is known for controlling SC quiescence, hair cycle progression, HF cell differentiation, and migration and differentiation in wound healing (Botchkarev, 2003; Kandyba et al., 2013; Kobielak et al., 2003; Lewis et al., 2014a, 2014b; Rendl et al., 2008; Zhang et al., 2015). Thus, an increase in BMP signaling could potentially explain, at least in part, the skin phenotypes induced by blocked hypomethylation at late Anagen/Catagen. BMP4 protein levels and histone methylation levels, were examined in normal skin by western blots at several key hair cycle stages (Figures 6A and S5A). At the onset of HFSC quiescence (late Anagen/Catagen, PD35-39), methylation decreases while BMP4 increases. When HFSC are activated (Telogen/Anagen, PD49-62), a reversed negative correlation occurs, when methylation increases and BMP4 decreases (Figure 4A). Interestingly, we noticed a positive correlation in the late stages of quiescence (Catagen/Telogen, PD44-49), where both methylation and BMP4 expression increased (Figures 6A and S5A). Significantly, DI-treated skin (e.g., with elevated methylation) showed an increase in BMP4 protein levels by western blots at all stages analyzed (Figures 6A and S5A). The *Bmp4* mRNA was also increased as shown by qRT-PCR of total skin at Catagen (Figure 6B). Wild-type bulge and non-bulge basal cells, FACS sorted as CD34+/α6-integrin+ and CD34−/α6-integrin+ cells, showed elevated expression of *Bmp4* at Catagen and Telogen relative to Anagen (Figure S5B), suggesting that the epithelial SCs are one source of BMP signals. Staining for BMP4 protein expression showed increased signal both in the CD34+ HFSCs and in the BL epidermis in DI-treated skin (Figures 6C, 6D, and S5C).

To understand how increasing the histone methylation levels may elevate BMP4, we began by analyzing the status of H3 K4/9/27me3 at the *Bmp4* gene locus using our previous chromatin immunoprecipitation (ChIP) sequencing results of sorted bulge HFSCs and non-bulge cells at Anagen and Catagen (Lee et al., 2016). Interestingly, transcription repression marks H3 K9/27me3 were removed from the *Bmp4* gene and promoter in the HFSCs by Catagen, while the transcription activation mark H3 K4me3 was considerably kept (Figure S5D). This was consistent with elevated expression of BMP4 at late quiescence stages in the epithelial cells (Figure 6A, 5B, and S5B). Next, we performed ChIP analysis of DI-treated skin at Anagen and Catagen to probe the level of H3 K4/9/27me3 marks on three *Bmp4* promoter regions previously shown to be functionally relevant for its expression (Figure 6E) (Zhang et al., 2015). The repressive marks (H3 K27me3 and H3 K9me3) were decreased in control mice at Catagen when compared with Anagen, as expected. However, they did not significantly change on promoter regions 1 and 2 in response to DI treatment. In contrast, promoter region 3 showed an increase in the

(D) Representative images of the shaved mouse back skin at different ages after applying CT or DI (PD35-42). Number of mice in each age is indicated in (C).
(E) Western blots for CT- or DI-treated mice during Anagen (PD28-35) phase show no differences in methylation levels. In contrast, application at PD35-42 induces prominent differences (1C, 1D, S1A, and S1B).
(F) Quantification of the western blots in (E) and additional blots in Figure S4A (N = 3 mice/group).
(G) Whole view of mouse back skin at PD98 after applying CT or DI at the time points indicated on the left. Note the normal hair growth in the top panels and delayed hair growth in the bottom right panels.
(H and I) Skin sections of CT- or DI-treated mice (PD35-42 induction scheme) at PD98 or PD129 show HFs with distinct morphology (H) and patterns of marker staining (I). The white arrowhead indicates an AE13+/Ki67+ cell.
(J) Quantification of the AE13 signal intensity/cell. N = 3; *p < 0.0001.
(K) Quantification of the Ki67+ cells in AE13+ cells in (I). N = 3; *p < 0.0001.
Student's t test was used for all significance tests. All experiments were executed twice. Scale bars, 20 μm.

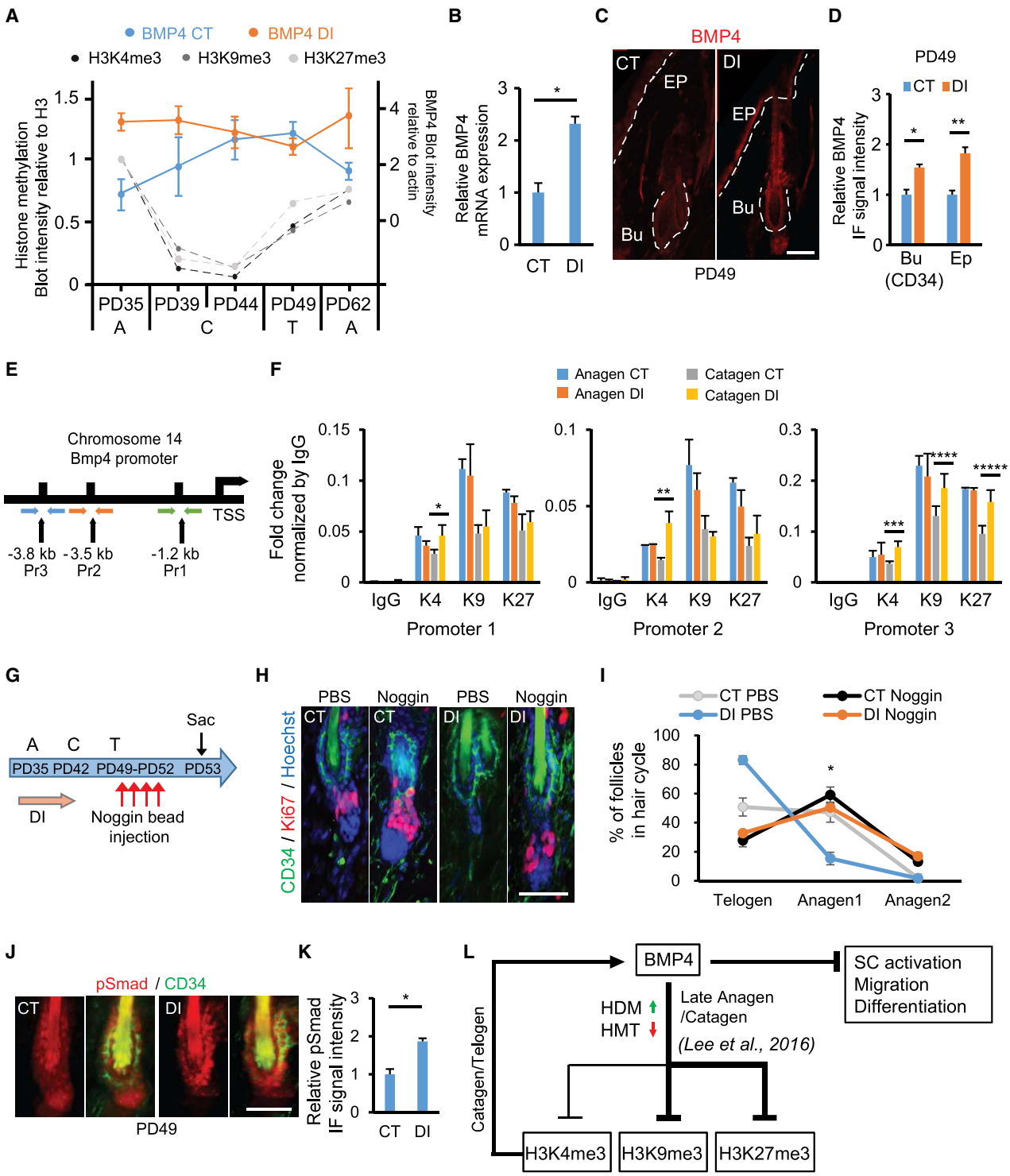

Figure 6. BMP4 Expression Is Increased by Blocking Hypomethylation at Late Anagen/Catagen

(A) Intensity graph of BMP4 normalized by β-actin of CT-treated (blue) or DI-treated (red) mice at late Anagen/Catagen extracted from western blots in Figure S5A at the ages and stages indicated. N = 2 for PD35; N = 3 for other ages. A, Anagen; C, Catagen; T, Telogen. Corresponding histone methylation levels normalized by H3 of CT-treated mice total skin at various ages are shown in gray and were extracted from Lee et al. (2016). Note the decrease in histone methylation level from Anagen to Catagen transition, accompanied by an

(legend continued on next page)

activating mark H3 K4me3 at Catagen in DI-treated skin (Figure 6F). These data together suggest that despite global inhibition of H3 K4/9/27me3 demethylases, *Bmp4* promoter regions are selectively demethylated, generally retaining H3 K4me3 and losing the H3 K9/K27me3. This selective pattern is not common throughout the genome, as demonstrated in a control tested gene (Figure S5E). These results could explain the observed increase of *Bmp4* mRNA and protein expression in DI-treated skin with blocked hypomethylation.

To confirm that the BMP signaling is hyperactive after applying DIs, we performed a rescue experiment using NOGGIN, which is a well-known BMP antagonist in skin (Plikus et al., 2008). After injecting the recombinant mouse NOGGIN in DI-treated skin, the hair cycle delay phenotype was rescued when compared with control PBS injected skin where follicles were still in Telogen (Figures 6G–6I and S5F). Furthermore, to investigate if increased BMP4 levels in DI-treated skin affects the BMP signaling, we analyzed the DI-treated skin with phosphorylated SMAD 1/5/9, which is a reporter of canonical BMP signaling (Botchkarev, 2003). Indeed, we observed increased pSMAD signal in the CD34+ HFSCs (Figures 6J and 6K). Normally pSMAD staining disappears when the HFs enter Anagen (Genander et al., 2014). However, pSMAD signal was still maintained in the DI-treated HFs adjacent to the wound (Figure S5G). This coincides with our results that spreading of the hair activation signals from the wound is more restricted in DI-treated skin (Figure 5B). Together, these data suggest that the canonical BMP pathway is hyperactive after blocking the hypomethylation during the Anagen/Catagen phase, because of selective targeting of the *Bmp4* promoter and increased BMP4 levels in the skin.

DISCUSSION

Here, we demonstrate an impact of global histone H3 K4/9/27me3 levels in SC dynamics and cell fate decision during adult skin regeneration: hair cycle and wound healing. Hypomethylation of histone H3 K4/9/27me3 and HFSC quiescence occur concomitantly at late Anagen/Catagen (Lee et al., 2016). We briefly interfere with the H3 K4/9/27me3 demethylases at this critical stage and identify remarkable long-term physiological effects on SC behavior in both HF and epidermis, along with impaired wound healing and defects in hair growth and differentiation. We show that chemical inhibition of demethylases is dependent on hair cycle stage. Finally, we implicate BMP4 as a downstream effector of hypomethylation that may at least in part explain these physiological effects. Our data provides a broad road map for future genetic studies of the control of H3 K4/9/27me3 levels in skin for proper hair growth and wound healing. We suggest possible pharmaco-chemical strategies to interfere with H3 K4/9/27me3 levels for future clinical studies.

Previously, we hypothesized that H3 K4/9/27me3 hypomethylation of HFSCs at Catagen was important for keeping the SCs in a highly plastic state of low epigenetic identity, such that HFSCs can easily adopt more differentiated cell fates in the subsequent stages of hair cycle (Kang et al., 2019; Lee et al., 2016). Our data here support this model, as inhibiting hypomethylation impairs the hair germ fate (this work), which is critical for HFSC activation (Greco et al., 2009), and also impairs proper HF differentiation to inner hair lineages (this work). It is remarkable that one week of DI treatment at a critical hair cycle stage can induce physiological effects in skin 60–80 days post-

increase in BMP4 levels. From Catagen to Telogen, histone methylation and BMP4 levels positively correlate, while from Telogen to Anagen, methylation continues to increase while BMP4 levels decrease.

(B) Gene expression analysis of *Bmp4* mRNA in CT- or DI-treated total back skin. N = 3 of biological replicates; *p = 0.018.

(C) Skin sections immunostained with BMP4 show expression of BMP4 in bulge and epidermis with apparent increase in DI-treated skin. Bu, bulge; Ep, epidermis.

(D) BMP4 fluorescence signal quantification in the bulge (CD34+ cells) and the basal layer cells as shown in Figure S5B. N = 3; *p = 0.022, **p = 0.003. Bu, bulge; Ep, epidermis.

(E) Scheme of the *Bmp4* promoter region with three primer sets upstream of the transcription start site (TSS) used for the P experiment of CT- or DI-treated skin.

(F) ChIP signal fold change of *Bmp4* promoter regions 1, 2, and 3 shown in (E). *p = 0.047, **p = 0.012, ***p = 0.029, ****p = 0.017, *****p = 0.04; N = 2 for Anagen (PD35) samples, N = 3 for Catagen (PD39) samples. The samples that were used for the ChIP experiments were the total skin samples of biological replicates after applying DI or control vehicles (CT).

(G) Scheme of the NOGGIN-coated bead injection experiment after applying DI.

(H) Skin sections immunostained with CD34 and Ki67 from mice sacrificed at PD53 after injecting NOGGIN in DI-treated skin.

(I) Quantification of the HFs in each hair cycle from (H). N = 3; *p = 0.014.

(J) Skin sections immunostained with CD34 and pSMAD1, 5, 9 at PD49 after applying DI at PD35-42.

(K) Quantification of fluorescence signals of pSMAD1, 5, 9 in the bulge (CD34+ cells) as shown in (J). N = 3; *p = 0.004.

(L) Working model describing histone methylation level crosstalk with BMP4.

Student's t test was used for all significance test. All experiments were executed twice. Scale bars, 20 μm.

treatment. In this critical stage histone demethylases must be highly active, explaining the hypomethylation and as demonstrated by the time-selective response to DIs. H3 K4/9/27me3 methylases are also downregulated at this stage relative to Anagen (Lee et al., 2016 and this work). Whereas at Catagen HFSC are hypomethylated and highly plastic, at Anagen they are likely in a state of high epigenetic identity, or a "rigid" stem cell fate state that promotes self-renewal (Lee et al., 2016). At late Anagen/Catagen hypomethylation occurs and is maintained all through Catagen, to provide flexibility of fate acquisition for HFSCs subsequent fates. Blocking hypomethylation at late Anagen/Catagen results in persistence of the Anagen HFSC epigenetic state, a highly methylated rigid-SC state, which then limits HFSC genome plasticity in subsequent stages and results in transient defects in activation and differentiation.

Skin punch regeneration is another measure of HFSC plasticity, since they migrate upward and trans-differentiate to IFE (Aragona et al., 2017; Ito et al., 2005; Jaks et al., 2008; Levy et al., 2007; Mascre et al., 2012). We demonstrate by lineage tracing that hypomethylation is necessary for subsequent contribution of both HF (*Lgr5*-CreER) and IFE (*Aspm*-CreER) SCs to wound healing. We describe the *Aspm*-CreER as a newfound genetic tool to mark the IFE SCs specifically, away from the HF lineages. The *Aspm*-CreER mice have been previously generated (Marinaro et al., 2011), but have not yet been studied in skin to our knowledge. Whereas HFSC contribution to epidermis repair has been intensively studied (Aragona et al., 2017; Ito et al., 2005; Jaks et al., 2008; Levy et al., 2007; Mascre et al., 2012), the contribution of epidermis to HFSCs upon injury has been more difficult, due to lack of specific and efficient genetic-labeling tools for the IFE. *De novo* HF regeneration from IFE SCs has been documented in severe injuries, such as very large skin excision or punch wounds (Ito et al., 2007; Plikus et al., 2015). With the *Aspm*-CreER-labeling tools, we demonstrate essentially no IFE cell migration to HF during normal homeostasis or in hair plucking, which then occurs specifically only near punch wound sites. It is possible that the IFE cells adopt new fates near the injury site, which may explain why H3 K27me3 mark is hypomethylated near wound edges (Shaw and Martin, 2009). More experiments are needed to understand if the IFE migrated cells actually contribute to HF growth, and whether methylation levels affect this process.

Interestingly, hypomethylation affected selectively epidermal cell differentiation and blood vessel recruitment in wound healing, but not epidermal cell proliferation and fibroblast recruitment. Our data suggest that a state of skin hypomethylation prior to injury may be beneficial to wound healing, as also suggested by low H3 K27me3 mark at the wound edge due to decreased PRC2 complex genes (*Ezh2* and *Eed*) and increased H3 K27me3 demethylases (*Utx* and *Jmjd3*) (Shaw and Martin, 2009). Hypomethylation of H3 K27me3 may be critical during wound healing, since injury-related genes, such as *Myc*, *Egfr* and *Mmp*s are de-repressed by loss of H3 K27me3 mark (Na et al., 2016; Shaw and Martin, 2009). Moreover, depletion of *Jmjd3* fails to activate epidermal differentiation-related genes in human keratinocytes (Sen et al., 2008). Previously, double knockout of *Ezh1/2* and loss of H3 K27me3 resulted in hyperproliferation in the BL of the epidermis in uninjured skin (Ezhkova et al., 2011). We have not observed a noticeable phenotype in the proliferation of the BL cells possibly due to compounding effects of H3 K7me3 with K4/9me3. This may point to complex interactions among various histone methyl marks that warrant further investigation.

Finally, despite global demethylase inhibition, we find that gene promoters are targeted differentially, with a selective upregulation of activating mark H3 K4me3 on the *Bmp4* promoter. BMP signaling may explain at least in part our phenotypes, given its known role in controlling SC quiescence, hair cycle progression, HF cell differentiation, and keratinocyte migration and differentiation in wound healing (Botchkarev, 2003; Kandyba et al., 2013; Kobielak et al., 2003; Lewis et al., 2014a; Rendl et al., 2008; Zhang et al., 2015). Interfering with BMP via NOGGIN injection rescued the hair cycle phenotype, adding to this model. Nevertheless, BMP is extremely unlikely the only pathway at play in the interface with histone methylation levels, and much more genomic work is required for a more comprehensive map of the pathways at play. BMP ligand expression is low at Anagen and increases at late Anagen/Catagen and throughout Telogen (this work) (Botchkarev and Sharov, 2004; Lee and Tumbar, 2012; Plikus et al., 2008). This BMP increase is accompanied by HFSCs hypomethylation along with decreased expression of histone methylases, such as *Setd1b* (H3 K4me3), *Suv39h2* (H3 K9me3), and *Ezh2* (H3 K27me3) (Lee et al., 2016), decreased proliferative signals and HFSC quiescence (Hsu et al., 2014; Kandyba et al., 2013; Lien et al., 2014; Plikus et al., 2008) (Figure 6A). Importantly, hypomethylation of H3 K4me3 was the mildest among the three different marks that decrease at Catagen (Lee et al., 2016), with significant levels retained on the *Bmp4* promoter (this work). Although our previous data suggested that BMP may be upstream promoting hypomethylation (Lee et al., 2016), we find here what may be a negative feedback loop in which hypomethylation may dampen the level of BMP4, primarily through maintaining H3 K4me3 levels (Figure 6L). We propose a working model for further investigation, in which a two-way dynamic feedback occurs between H3 K4/9/27 trimethylation and BMP signaling during different stages of the hair cycle (Figure 6L).

Altogether, our data using chemical inhibition of demethylases in skin provides a broad picture of how overall global histone H3 K4/9/27me3 levels can affect hair homeostasis and skin injury repair for future genetic testing and clinical applications.

EXPERIMENTAL PROCEDURES

Mice, Histone DI Administration and Noggin Injection

All mice were treated according to Cornell University Institutional Animal Care and Use Committee protocols. Both males and females were used for all of the experiments, and were sex matched for Control (CT) and experimental groups. For applying DIs, GSK J1 (no. 4593, Tocris) and JIB 04 (no. 4972, Tocris) were dissolved in dimethylsulfoxide at 100 mM and then diluted in 100% acetone to the final concentration of 500 μM. CD1 × FVB littermates back skin was shaved and 100 μL of inhibitors were topically applied on the shaved regions every 12 hr for indicated periods (Figures 1B and 5C). Control mice received only dimethylsulfoxide in acetone. For Noggin-coated bead injection, we followed a method described previously (Lee et al., 2016). In brief, small regions of the DI-treated mice back skin was carefully clipped to avoid injury. Recombinant mouse Noggin (5 μg mL^{-1}, 1967-NG-025 R&D Systems) was incubated with FluoSpheres (Invitrogen) for 30 min at room temperature, and injected intradermally for 4 consecutive days in the same region. Control sides were injected PBS only.

Western Blot

For protein detection, we used mouse back skin which was harvested, snap frozen in liquid nitrogen and grated in the mortar. For Figures 6A and S5A, DI was treated at PD32-35 for PD35 samples and PD32-39 for PD39 samples. For the rest of the samples, DI was treated at PD35-42. All of the samples were lysed in RIPA buffer (10 mM Tris-Cl [pH 8.0], 1 mM EDTA, 1% Triton X-100, 0.1% sodium deoxycholate, 0.1% SDS, 140 mM NaCl, 1 mM PMSF). The protein was detected using antibodies-H3 (1:5,000, ab1791, Abcam), H3 K4me3 (1:5,000, no. 39159, Active Motif), H3 K9me3 (1:5,000, ab8898, Abcam), H3 K27me3 (1:5,000, no. 07–449, Millipore), β-actin (1:2,000, MAB1501MI, Millipore), and BMP4 (1:1,000, ab39973, Abcam). ImageJ (http://imagej.nih.gov/ij/) was used for quantification of the blot intensity.

Immunofluorescence Staining

The tissue immunofluorescence staining method has been described previously (Lee et al., 2016). Antibodies of H3 K4me3 (1:1,000, no. 39159, Active Motif), H3 K9me3 (1:2,000, ab8898, Abcam), H3 K27me3 (1:2,000, no. 07-449, Millipore), CD34 (1:200, no. 553731, BD Biosciences), mouse α-K14 (1:100, ab7800, Abcam), Ki67 (1:500, ab15580, Abcam), AE13 (1:50, IQ292, ImmuQuest), BMP4 (1:200, ab39973, Abcam), K1 (1:200, PRB165P, Covance), K10 (1:100, PRB159P, Covance), CD31 (1:200, no. 550274, BD Biosciences), Tenascin (1:500, AB19013, Millipore), pSmad1 (S463/465), 5 (S463/465), 9 (S465/467) (1:100, 13820S Cell Signal), and Vimentin (1:1,000, a gift from Dr. Yan Lammerding, Cornell University) were used.

qRT-PCR and FACS

For FACS sorting of HFSCs and BL cells, the protocol has been described previously (Lee et al., 2016). The epithelial cells were isolated from the back skin through trypsin digestion. The cell suspensions were labeled with anti-CD34-Biotin (1:50, no. 13-0341-85, eBioscience), α-Streptavidin-APC (1:100, no. 554067, BD Biosciences) and anti-α6-integrin-PE (1:40, CD49f, no. 555736, BD Biosciences) to isolate HFSCs (CD34+, α6-integrin+) and BL cells (CD34−, α6-integrin+). Propidium iodide (1:1,250–1:2,500 of 1 mg mL^{-1} stock, S7109, Sigma) was used to rule out the dead cells. For negative controls to gate the fluorescence-labeled cells, we used only α-Streptavidin-APC for CD34+ cells and PE-Rat-IgG2a (1:40, no. 555844, BD Biosciences) for α6-integrin+ cells. The cells were isolated with BD FACSAria located in the Flow Cytometry Core at Cornell University.

For gene expression analysis, RNA was extracted from either 1 cm^2 of total skin using the RNeasy Fibrous Tissue Mini Kit (no. 74704, QIAGEN) or the FACS-sorted cells using the mirVana miRNA Isolation Kit (AM1591, Ambion). The cDNA were synthesized using iScript (no. 1708841, Bio-Rad) cDNA synthesis kit and qRT-PCR analysis was described previously (Lee et al., 2016).

ChIP

For ChIP analysis, we used 1 cm^2 of CT- and DI-treated mice total skin as described previously (Lee et al., 2016). DI was applied from PD32-35 for Anagen PD35 samples and PD32-39 for Catagen PD39 samples. Two micrograms of each H3 (ab1791, Abcam), H3 K4me3 (no. 39159, Active Motif), H3 K9me3 (ab8898, Abcam), H3 K27me3 (no. 07-449, Millipore), and IgG (ab18413, Abcam) were used for immunoprecipitation. Purified DNA samples were analyzed by qRT-PCR with *Bmp4* and *Wnt4* promoter targeting primers. The primers are listed in Table S1.

Hair Plucking Experiments

For hair plucking, a hair removal sugar wax kit (Emerita) was used. *Aspm*-CreER;Rosa26 tdTomato mice were injected with 10 μg μL^{-1} of TM (200 μg g^{-1} body) at PD49. Then they were anesthetized and back skin hair was gently shaved (to avoid injury and unwanted hair growth activation) at PD70. A warm hair removal wax was applied to right side of back skin with a paper strip, and removed after 30 s. The wounded tissues were harvested after 2 weeks and 1 month.

Punch Wound Biopsy, *Ex Vivo* Biopsy Culture and Lineage Tracing Experiments

For all wounds 4 mm of disposable biopsy punches (no. 33-34, Integra Miltex) were used. PD49 mice were shaved and their back skin punch wounded, as described (Ge et al., 2017), then sacrificed at different time points.

For lineage tracing experiments, *Lgr5*-CreER;Rosa26 tdTomato (Jackson Laboratory) and *Aspm*-CreER;Rosa26 tdTomato transgenic mice (Madisen et al., 2010; Marinaro et al., 2011) were used. First, these mice were injected with 10 μg μL^{-1} of TM (200 μg g^{-1} body). Then, GSK J1 (no. 4593, Tocris) and JIB 04 (no. 4972, Tocris) dissolved vehicles were applied on the back

skin for a week. The wounded tissues were harvested after 1, 3, and 5 weeks after the punch wound.

Microscopy

For Figures 1H, 3G, 4C, and S1F, tissue samples were analyzed by confocal microscopy (Zeiss LSM710) with Zen 2012 software. Projected z stack images are viewed from the basal surface with stitched tiled images.

Otherwise we used a widefield fluorescence light microscope (Nikon) equipped with a charge-coupled device 12-bit digital camera (Retiga EXi; QImaging). For Figures 1G, 1I, 3E, 5B, and S1C–S1E, images were taken individually and stitched together as a whole image.

Statistical Analysis

All values were shown as mean ± SD. At least 3 mice ($n > 100$ cells) were taken from each group for significant test (e.g., Student's t test and ANOVA for Figures 1F and 3D) where $p < 0.05$ was considered significant. For Figures 1F and 3D, ANOVA significant test was performed using JMP software.

SUPPLEMENTAL INFORMATION

Supplemental Information can be found online at https://doi.org/10.1016/j.stemcr.2019.11.007.

AUTHOR CONTRIBUTIONS

S.K. and T.T. designed the experiments. K.L. repeated the experiments in Figure 5G and performed tissue staining in Figures 5I and S4C, and analyzed the quantifications in Figures 5J, 5K, and S4B. S.W. performed some of the hair-plucking analysis. A.S. performed lineage tracing with Aspm-CreER/Rosa26-tdTomato mice in normal skin homeostasis. S.K. performed the rest of the experiments and prepared the figures. S.K. and T.T. wrote the manuscript.

ACKNOWLEDGMENTS

We thank Jayhun Lee for help with ChIP sequencing data retrieval from original database. S.K. has been supported in part by a training grant from the Cornell VERGE. The work was supported by NIH NIAMS RO1 AR070157 and AR073806 grants to T.T.

Received: January 23, 2019
Revised: November 20, 2019
Accepted: November 21, 2019
Published: December 19, 2019

REFERENCES

Aragona, M., Dekoninck, S., Rulands, S., Lenglez, S., Mascre, G., Simons, B.D., and Blanpain, C. (2017). Defining stem cell dynamics and migration during wound healing in mouse skin epidermis. Nat. Commun. *8*, 14684.

Avgustinova, A., and Benitah, S.A. (2016). Epigenetic control of adult stem cell function. Nat. Rev. Mol. Cell Biol. *17*, 643–658.

Baxter, J., Sauer, S., Peters, A., John, R., Williams, R., Caparros, M.L., Arney, K., Otte, A., Jenuwein, T., Merkenschlager, M., et al. (2004). Histone hypomethylation is an indicator of epigenetic plasticity in quiescent lymphocytes. EMBO J. *23*, 4462–4472.

Blanpain, C., and Fuchs, E. (2014). Stem cell plasticity. Plasticity of epithelial stem cells in tissue regeneration. Science *344*, 1242281.

Botchkarev, V.A. (2003). Bone morphogenetic proteins and their antagonists in skin and hair follicle biology. J. Invest. Dermatol. *120*, 36–47.

Botchkarev, V.A., and Sharov, A.A. (2004). BMP signaling in the control of skin development and hair follicle growth. Differentiation *72*, 512–526.

Boyer, L.A., Plath, K., Zeitlinger, J., Brambrink, T., Medeiros, L.A., Lee, T.I., Levine, S.S., Wernig, M., Tajonar, A., Ray, M.K., et al. (2006). Polycomb complexes repress developmental regulators in murine embryonic stem cells. Nature *441*, 349–353.

Chen, J., Liu, H., Liu, J., Qi, J., Wei, B., Yang, J., Liang, H., Chen, Y., Chen, J., Wu, Y., et al. (2013). H3K9 methylation is a barrier during somatic cell reprogramming into iPSCs. Nat. Genet. *45*, 34–42.

Ezhkova, E., Lien, W.H., Stokes, N., Pasolli, H.A., Silva, J.M., and Fuchs, E. (2011). EZH1 and EZH2 cogovern histone H3K27 trimethylation and are essential for hair follicle homeostasis and wound repair. Genes Dev. *25*, 485–498.

Fuchs, E. (2009). The tortoise and the hair: slow-cycling cells in the stem cell race. Cell *137*, 811–819.

Ge, Y., Gomez, N.C., Adam, R.C., Nikolova, M., Yang, H., Verma, A., Lu, C.P., Polak, L., Yuan, S., Elemento, O., et al. (2017). Stem cell lineage infidelity drives wound repair and cancer. Cell *169*, 636–650.e14.

Genander, M., Cook, P.J., Ramskold, D., Keyes, B.E., Mertz, A.F., Sandberg, R., and Fuchs, E. (2014). BMP signaling and its pSMAD1/5 target genes differentially regulate hair follicle stem cell lineages. Cell Stem Cell *15*, 619–633.

Greco, V., Chen, T., Rendl, M., Schober, M., Pasolli, H.A., Stokes, N., Dela Cruz-Racelis, J., and Fuchs, E. (2009). A two-step mechanism for stem cell activation during hair regeneration. Cell Stem Cell *4*, 155–169.

Hawkins, R.D., Hon, G.C., Lee, L.K., Ngo, Q., Lister, R., Pelizzola, M., Edsall, L.E., Kuan, S., Luu, Y., Klugman, S., et al. (2010). Distinct epigenomic landscapes of pluripotent and lineage-committed human cells. Cell Stem Cell *6*, 479–491.

Hsu, Y.C., Pasolli, H.A., and Fuchs, E. (2011). Dynamics between stem cells, niche, and progeny in the hair follicle. Cell *144*, 92–105.

Hsu, Y.C., Li, L., and Fuchs, E. (2014). Emerging interactions between skin stem cells and their niches. Nat. Med. *20*, 847–856.

Ito, M., Liu, Y., Yang, Z., Nguyen, J., Liang, F., Morris, R.J., and Cotsarelis, G. (2005). Stem cells in the hair follicle bulge contribute to wound repair but not to homeostasis of the epidermis. Nat. Med. *11*, 1351–1354.

Ito, M., Yang, Z., Andl, T., Cui, C., Kim, N., Millar, S.E., and Cotsarelis, G. (2007). Wnt-dependent de novo hair follicle regeneration in adult mouse skin after wounding. Nature *447*, 316–320.

Jaks, V., Barker, N., Kasper, M., van Es, J.H., Snippert, H.J., Clevers, H., and Toftgard, R. (2008). Lgr5 marks cycling, yet long-lived, hair follicle stem cells. Nat. Genet. *40*, 1291–1299.

Jiang, H., Shukla, A., Wang, X., Chen, W.Y., Bernstein, B.E., and Roeder, R.G. (2011). Role for Dpy-30 in ES cell-fate specification by regulation of H3K4 methylation within bivalent domains. Cell *144*, 513–525.

Kandyba, E., Leung, Y., Chen, Y.B., Widelitz, R., Chuong, C.M., and Kobielak, K. (2013). Competitive balance of intrabulge BMP/Wnt signaling reveals a robust gene network ruling stem cell homeostasis and cyclic activation. Proc. Natl. Acad. Sci. U S A *110*, 1351–1356.

Kang, S., Chovatiya, G., and Tumbar, T. (2019). Epigenetic control in skin development, homeostasis and injury repair. Exp. Dermatol. *28*, 453–463.

Kobielak, K., Pasolli, H.A., Alonso, L., Polak, L., and Fuchs, E. (2003). Defining BMP functions in the hair follicle by conditional ablation of BMP receptor IA. J. Cell Biol. *163*, 609–623.

Kruidenier, L., Chung, C.W., Cheng, Z., Liddle, J., Che, K., Joberty, G., Bantscheff, M., Bountra, C., Bridges, A., Diallo, H., et al. (2012). A selective jumonji H3K27 demethylase inhibitor modulates the proinflammatory macrophage response. Nature *488*, 404–408.

Lee, J., Hoi, C.S., Lilja, K.C., White, B.S., Lee, S.E., Shalloway, D., and Tumbar, T. (2013). Runx1 and p21 synergistically limit the extent of hair follicle stem cell quiescence in vivo. Proc. Natl. Acad. Sci. U S A *110*, 4634–4639.

Lee, J., and Tumbar, T. (2012). Hairy tale of signaling in hair follicle development and cycling. Semin. Cell Dev. Biol. *23*, 906–916.

Lee, J., and Tumbar, T. (2017). Linking chromatin dynamics, cell fate plasticity, and tissue homeostasis in adult mouse hair follicle stem cells. Mol. Life *1*, 15–21.

Lee, J., Kang, S., Lilja, K.C., Colletier, K.J., Scheitz, C.J., Zhang, Y.V., and Tumbar, T. (2016). Signalling couples hair follicle stem cell quiescence with reduced histone H3 K4/K9/K27me3 for proper tissue homeostasis. Nat. Commun. *7*, 11278.

Levy, V., Lindon, C., Zheng, Y., Harfe, B.D., and Morgan, B.A. (2007). Epidermal stem cells arise from the hair follicle after wounding. FASEB J. *21*, 1358–1366.

Lewis, C.J., Mardaryev, A.N., Poterlowicz, K., Sharova, T.Y., Aziz, A., Sharpe, D.T., Botchkareva, N.V., and Sharov, A.A. (2014a). Bone morphogenetic protein signaling suppresses wound-induced skin repair by inhibiting keratinocyte proliferation and migration. J. Invest. Dermatol. *134*, 827–837.

Lewis, C.J., Mardaryev, A.N., Sharov, A.A., Fessing, M.Y., and Botchkarev, V.A. (2014b). The epigenetic regulation of wound healing. Adv. Wound Care (New Rochelle) *3*, 468–475.

Lien, W.H., Polak, L., Lin, M., Lay, K., Zheng, D., and Fuchs, E. (2014). In vivo transcriptional governance of hair follicle stem cells by canonical Wnt regulators. Nat. Cell Biol. *16*, 179–190.

Liu, L., Cheung, T.H., Charville, G.W., Hurgo, B.M., Leavitt, T., Shih, J., Brunet, A., and Rando, T.A. (2013). Chromatin modifications as determinants of muscle stem cell quiescence and chronological aging. Cell Rep. *4*, 189–204.

Loh, Y.H., Zhang, W., Chen, X., George, J., and Ng, H.H. (2007). Jmjd1a and Jmjd2c histone H3 Lys 9 demethylases regulate self-renewal in embryonic stem cells. Genes Dev. *21*, 2545–2557.

Madisen, L., Zwingman, T.A., Sunkin, S.M., Oh, S.W., Zariwala, H.A., Gu, H., Ng, L.L., Palmiter, R.D., Hawrylycz, M.J., Jones, A.R., et al. (2010). A robust and high-throughput Cre reporting and characterization system for the whole mouse brain. Nat. Neurosci. *13*, 133–140.

Marinaro, C., Butti, E., Bergamaschi, A., Papale, A., Furlan, R., Comi, G., Martino, G., and Muzio, L. (2011). In vivo fate analysis reveals the multipotent and self-renewal features of embryonic AspM expressing cells. PLoS One *6*, e19419.

Martin, P., and Leibovich, S.J. (2005). Inflammatory cells during wound repair: the good, the bad and the ugly. Trends Cell Biol. *15*, 599–607.

Mascre, G., Dekoninck, S., Drogat, B., Youssef, K.K., Brohee, S., Sotiropoulou, P.A., Simons, B.D., and Blanpain, C. (2012). Distinct contribution of stem and progenitor cells to epidermal maintenance. Nature *489*, 257–262.

Mattout, A., and Meshorer, E. (2010). Chromatin plasticity and genome organization in pluripotent embryonic stem cells. Curr. Opin. Cell Biol. *22*, 334–341.

Meshorer, E., Yellajoshula, D., George, E., Scambler, P.J., Brown, D.T., and Misteli, T. (2006). Hyperdynamic plasticity of chromatin proteins in pluripotent embryonic stem cells. Dev. Cell *10*, 105–116.

Na, J., Lee, K., Na, W., Shin, J.Y., Lee, M.J., Yune, T.Y., Lee, H.K., Jung, H.S., Kim, W.S., and Ju, B.G. (2016). Histone H3K27 demethylase JMJD3 in cooperation with NF-kappaB regulates keratinocyte wound healing. J. Invest. Dermatol. *136*, 847–858.

Plikus, M.V., Guerrero-Juarez, C.F., Treffeisen, E., and Gay, D.L. (2015). Epigenetic control of skin and hair regeneration after wounding. Exp. Dermatol. *24*, 167–170.

Plikus, M.V., Mayer, J.A., de la Cruz, D., Baker, R.E., Maini, P.K., Maxson, R., and Chuong, C.M. (2008). Cyclic dermal BMP signalling regulates stem cell activation during hair regeneration. Nature *451*, 340–344.

Rendl, M., Polak, L., and Fuchs, E. (2008). BMP signaling in dermal papilla cells is required for their hair follicle-inductive properties. Genes Dev. *22*, 543–557.

Sada, A., and Tumbar, T. (2013). New insights into mechanisms of stem cell daughter fate determination in regenerative tissues. Int. Rev. Cell Mol. Biol. *300*, 1–50.

Sada, A., Jacob, F., Leung, E., Wang, S., White, B.S., Shalloway, D., and Tumbar, T. (2016). Defining the cellular lineage hierarchy in the interfollicular epidermis of adult skin. Nat. Cell Biol. *18*, 619–631.

Sen, G.L., Webster, D.E., Barragan, D.I., Chang, H.Y., and Khavari, P.A. (2008). Control of differentiation in a self-renewing mammalian tissue by the histone demethylase JMJD3. Genes Dev. *22*, 1865–1870.

Shaw, T., and Martin, P. (2009). Epigenetic reprogramming during wound healing: loss of polycomb-mediated silencing may enable upregulation of repair genes. EMBO Rep. *10*, 881–886.

Wang, L., Chang, J., Varghese, D., Dellinger, M., Kumar, S., Best, A.M., Ruiz, J., Bruick, R., Pena-Llopis, S., Xu, J., et al. (2013). A small molecule modulates Jumonji histone demethylase activity and selectively inhibits cancer growth. Nat. Commun. *4*, 2035.

Zhang, Y., Yeh, L.K., Zhang, S., Call, M., Yuan, Y., Yasunaga, M., Kao, W.W., and Liu, C.Y. (2015). Wnt/beta-catenin signaling modulates corneal epithelium stratification via inhibition of Bmp4 during mouse development. Development *142*, 3383–3393.